sciendo
Austrian Journal of Earth Sciences | Vienna | 2020 | Volume 113/2 | 201 - 210 | DOI: 10.17738/ajes.2020.0012

# Conodont thermometry by Raman spectroscopy on carbonaceous material: a case study from the Northern Calcareous Alps (Mürzalpen Nappe, Eastern Alps)

Gerd RANTITSCH[1]*, Gerhard BRYDA[2], Hans-Jürgen GAWLICK[1]
[1)] Department für angewandte Geowissenschaften und Geophysik, Montanuniversität Leoben, Peter-Tunner Straße 5, 8700 Leoben, Austria;
[2)] Geologische Bundesanstalt Wien, Neulinggasse 38, 1030 Wien, Austria;
*) corresponding author: gerd.rantitsch@unileoben.ac.at

KEYWORDS
Northern Calcareous Alps, Greywacke Zone, Aflenz, Raman Spectroscopy, Conodont Color Alteration Index, Thermometry

**Abstract**
Carnian metapelites from the southeastern segment of the Mürzalpen Nappe (Northern Calcareous Alps, Eastern Alps) were heated to 280-310 °C, estimated by Raman spectroscopy of carbonaceous material (RSCM). This temperature range is correlated to a Color Alteration Index of 5.0-6.5, determined on conodonts from adjacent Anisian to Norian carbonates. Average RSCM temperatures estimated on the conodonts are biased towards higher temperatures. The spectral characteristics of the conodont apatite suggest a composition altered during progressive recrystallization, influencing the band parameters of the included carbonaceous matter. Consequently, accurate conodont RSCM thermometry needs an assessment of apatite alteration.

## 1 Introduction

Because of missing indicator minerals, the determination of valid peak temperatures of very low- to low-grade metamorphic carbonate rocks remains uncertain. As a common approach, applied in Paleozoic to Triassic carbonates, the color alteration of conodonts is interpreted as a result of burial heating and tectono-metamorphic processes. Here, the visually observed conodont color is assessed by the Color Alteration Index (CAI 1.0-8.0, scaled in 0.5 steps; Epstein et al., 1977; Rejebian et al., 1987). Based on experimental data and assuming a reasonable time scale for the thermal history, the CAI scale is correlated to rising metamorphic temperatures (Epstein et al., 1977; Rejebian et al., 1987). However, missing information about the burial and heat flow history of a carbonate sequence and the sensitivity of conodonts against diagenetic or hydrothermal modifications of their bioapatite material (e.g. Trotter and Eggins, 2006) challenges this application. Consequently, as an alternative to CAI investigations (Gawlick et al., 1994), metapelites intercalated in carbonate rocks of the Northern Calcareous Alps (Eastern Alps) were investigated by clay mineralogical (e.g. Schramm 1982; Kralik et al., 1987), organic petrological (e.g. Rantitsch and Russegger, 2005), and thermochronological methods (e.g. Kralik et al., 1987; Frank and Schlager, 2006) to get an estimate for the carbonates of the same stratigraphic level.

Marshall et al. (2001), Pucéat et al. (2004) and McMillan and Golding (2019) applied Raman spectroscopy on organic material (RSCM) included in conodont elements (Medici et al., 2020). McMillan and Golding (2019) concluded that the IFORS ('Interactive Fitting of Raman Spectra') approach of Lünsdorf et al. (2017) is able to estimate reliable burial temperatures of the host carbonates, corresponding to the related CAI temperatures. This approach is followed here to investigate the metamorphic imprint of Triassic carbonates of the Mürzalpen Nappe of the Northern Calcareous Alps (Linzer et al., 1995; Mandl, 2000). Investigating also metapelites of their metamorphic basement units, the goal is to reconstruct the thermal gradient in this section and to test the IFORS application on Triassic conodonts by the additional analysis of metapelites intercalated in the investigated host carbonates (McMillan and Golding, 2019). The study area (Figure 1) is located at the intensely heated (Kralik et al., 1987; Gawlick et al., 1994) southeastern margin of the Northern Calcareous Alps. Thus, as CAI values have been mapped for the entire unit (Gawlick et al., 1994), any valid correlation between RSCM temperatures and CAI may provide a way to estimate reliable metamorphic temperatures within this prominent tectonic unit of the Eastern Alps (Gawlick et al., 1999; Mandl, 2000).

## 2 Geological Setting

The study area (Figure 1) exposes a section through the Alpine nappe stack, attributed to the Upper Austroalpine tectonic unit of the Eastern Alps (Schmid et al., 2004). In the examined section, Eoalpine (early Late Cretaceous) metamorphic rocks of the Noric (Tirolic-Noric Nappe System), Silbersberg and Veitsch Nappes (parts of the Greywacke

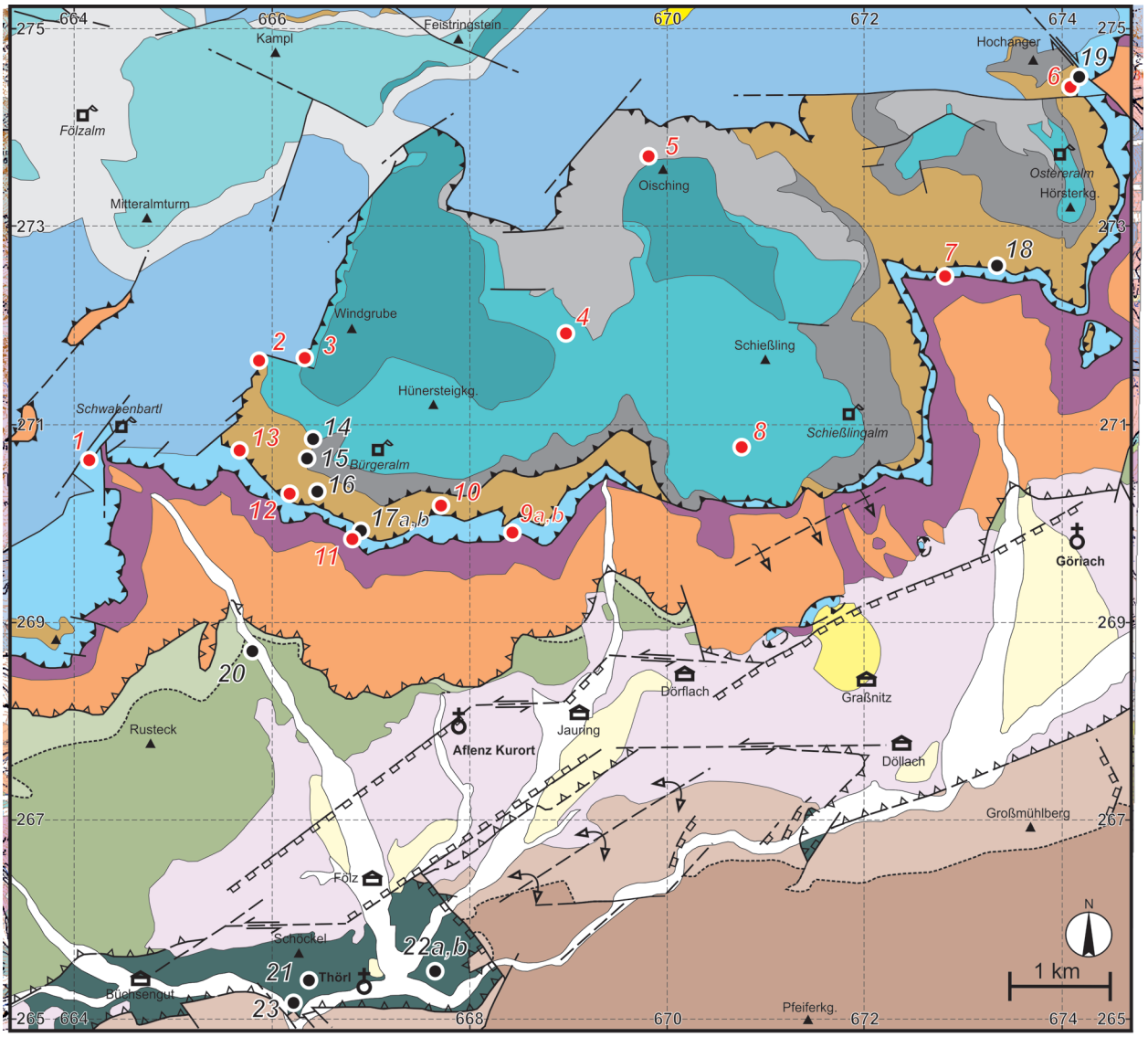


**Quaternary deposits**
- Alluvial deposits; Holocene
- Niederterrasse; Würm Glacial
- Moraine; Würm Glacial
- Slope sediment, loamy

**Intramontane basins**

Aflenz Basin (Miocene)
- Rud. clastics, coal, shale, diatomite

**Juvavic Nappe System**

Mürzalpen Nappe
- Dachstein Lmst.
- Waxeneck Dol.
- Aflenz Fm.
- Pötschen Lmst. and Dol.
- Mannsteinwald Fm.
- Jauring Fm.
- Leckkogel Fm.
- Wetterstein Lmst. and Dolomite
- Reifling and Grafensteig Fms.
- Anisian Dolomite, Steinalm Fm.
- Werfen Fm.

**Tirolic-Noric Nappe System**

Noric Nappe
- Permo-Mesozoic Cover
- Paleozoic Basement

▲ Peak  Village

Church  Alpine hut

**Greywacke Zone Nappe System**
- Silbersberg & Veitsch Nappe

**Silvretta Seckau Nappe System**

Troiseck-Floning Nappe
- Permo-Mesozoic Cover
- Crystalline Basement

1 14 **Conodont** & **rock** sample points

Unconformity  Fault (c., i.)

Normal fault (certain, inferred)

Strike-slip fault (cetain, inferred)

Nappe boundary (certain, inferred)

Thrustplane (certain, inferred)

Anticline, Monocline

**Figure 1:** Study area (redrawn from Bryda et al., 2020) and sample locations ((Dol = dolomite, Lmst = limestone, Rud. clastics= rudist-clastic sediments; coordinates in the Austrian BMN system, EPSG 31286)).

Zone Nappe System) are overlain by the Mürzalpen Nappe (Juvavic Nappe System of the Northern Calcareous Alps) predominately composed of carbonate rocks (Bryda et al., 2020). The studied section is overstepped by alluvial, fluviatile and lacustrine sediments of the Miocene Aflenz Basin, which subsided in a pull-apart setting along the Mur-Mürz fault system (Sachsenhofer et al., 2003).

At the bottom of the section, Variscan amphibolite-facies metamorphic basement rocks of the Troiseck-Floning Nappe (Schuster and Nowotny, 2015) are covered by post-Variscan (Permian-Triassic) sediments, overprinted by Cretaceous (Eoalpine) metamorphism (Dallmeyer et al., 1998). Tectonically above, the Veitsch Nappe comprises Upper Carboniferous carbonates and siliciclastics (Ratschbacher, 1987). This nappe is overlain by quartzphyllites and Permian metaclastics of the lateral discontinuous Silbersberg Nappe (Neubauer et al., 1994). The following Noric Nappe is composed of Middle Ordovician to Upper Carboniferous volcanics, carbonates and metasediments (Neubauer et al., 1994) and transgressive Permian (Prebichl Formation) to Lower Triassic (Werfen Formation) sediments. The Noric Nappe (Tirolic-Noric Nappe System) is the basement unit of the basal Northern Calcareous Alps. The Mürzalpen Nappe, as part of the tectonically high Juvavic Nappe System, is at the top.

The Mürzalpen Nappe (Figure 1) is composed predominantly of 2 to 2.5 km thick limestones and dolomites, attributed to the Steinalm Carbonate Ramp, to the Wetterstein Platform, and to the Dachstein Platform (Mandl, 2001; Lein, 2010; Bryda et al., 2013). At the basal thrust, isolated bodies of Upper Permian evaporites (Haselgebirge) and Lower Triassic shallow water siliciclastics (Werfen Formation) are outcropping. They form the tectonic base of Middle to Late Triassic shallow-water to basinal sequences, exposing carbonate ramp deposits (Steinalm Formation), followed by the basinal Reifling and Grafensteig Formations and later by slope and platform carbonates (fore-reefal/reefal to lagoonal Wetterstein Formation; Bryda et al., 2013). After the demise of the Wetterstein Platform in the "Middle Carnian", the platform top was covered by a thin sequence of dark shales, fine-grained sandstones and dark and bedded limestones. At the same time, pelites (Reingraben slate i.e. Halobian slate), allodapic limestones, dolomites and rud-/floatstones (slope sediments) were deposited in a basin at the southeastern rim of the platform (Upper Triassic Aflenz Basin; Lein, 2010 and references therein). The mixed siliciclastic-carbonaceous sedimentary rocks in the basin and at the top of the carbonate platform are members of the Leckkogel Formation (Lein, 2010). In the Late Carnian, intense carbonate production started again. At the slope of the Aflenz Basin, during the Late Carnian to Middle Norian, thin bedded allodapic dolomites and thick dolomitic breccias were deposited (Mannsteinwald Formation; Figure 1), followed by grey siliceous deep-water limestones of Late Norian to Early Rhaetian age. This Late Triassic sequence is interpreted as transitional part between the allodapic limestone succession of the distal basin part (Jauring Formation and Pötschen Limestone; Bryda et al., 2020) and the Norian-Rhaetian Dachstein Platform (lagoon, reef and proximal slope).

The nappe stack below the Mürzalpen Nappe was metamorphosed at upward decreasing greenschist-facies metamorphic conditions (ca. 300–450 °C) during Eoalpine (80-100 Ma) thrust tectonics (Dallmeyer et al., 1998). Applying RSCM, Rantitsch et al. (2004) estimated metamorphic temperatures of 330-400 °C for the Veitsch Nappe. West of the study area, at the Erzberg region, 240-350 °C were determined for rocks of the Noric Nappe (Frühauf, 2017) using the same methodology. Well-constrained temperature estimates for the Mürzalpen Nappe are however missing. Anchizonal illite crystallinity values and a vitrinite reflectance of 1.6-2.5 %Ro characterize Upper Permian sediments (Haselgebirge) at the base of the Mürzalpen Nappe, heated to more than 160 °C (Spötl and Hasenhüttl, 1998). The corresponding maximum temperature of 255-353 °C is determined west of the study area by the presence of polyhalite in the Haselgebirge (Leitner et al., 2014). This is in accordance to sulfur isotope thermometry yielding 280-360 °C (Bojar et al., 2018). CAI values > 5.5 suggest temperatures of 300-480 °C in the Triassic carbonates of the Mürzalpen Nappe (Gawlick et al., 1994; Lein and Gawlick, 2001). This high degree of metamorphism is explained by a former external position of the Mürzalpen Nappe (part of the outer shelf; Gawlick et al., 1999; Mandl, 2000) at the Austroalpine Neo-Tethys continental margin, which was destroyed by Late Jurassic (Schuster and Frank, 1999; Frisch and Gawlick, 2003; Frank and Schlager, 2006; Haas et al., 2020) and early Late Cretaceous (Eoalpine) tectonics (Frank and Schlager, 2006).

## 3 Samples and methods

Conodonts of 14 Anisian-Norian carbonate samples (limestones, dolomites) from the Mürzalpen Nappe were investigated (Figure 1, Table 1). Carbonates were solved in acidic acid (ca. 8 %) to avoid any influence on the conodont apatite by the solving process. Residue was dried with max. 80 °C to avoid any influence on the CAI or internal structure of conodonts. Age ranges of the conodonts are given according to Budurov and Sudar (1990), Noyan and Kozur (2007), Krystyn et al. (2009), Orchard (2010), and Chen et al. (2016), using the nomenclature of Budurov and Sudar (1990), Gallet et al. (1998), and Krystyn et al. (2009). Slates intercalated in Anisian-Norian carbonates (Carnian Leckkogel Formation) were sampled in seven localities (Figure 1, Table 2). The sample set is completed by five samples from the tectonically lower Noric and Veitsch Nappes (Figure 1, Table 2).

Carbonaceous matter from the metapelite samples was isolated by an acid treatment. To keep the specimens undestroyed and to avoid any mechanical stress, which may influence the Raman spectra, conodonts were not sectioned prior to analysis as performed by McMillan and Golding (2019) and analyzed directly on the element surface. Thus, the estimated peak parameters are related to the surface characteristics of the conodont specimens.

**Table 1:** Conodont samples (coordinates in the Austrian BMN system, EPSG 31286) and Color Alteration Index (CAI).

| Sample | X | Y | Genus/Species | Age | CAI |
|---|---|---|---|---|---|
| | | | **Pötschen Limestone (Late Carnian-Middle Norian)** | | |
| 2 | 665896 | 271654 | *Paragondolella polygnathiformis* | Tuvalian | 5.5 |
| 3 | 666349 | 271681 | *Epigondolella rigoi, Epigondolella quadrata* | Lacian1 | 5.0-5.5 |
| 4 | 668984 | 271923 | *Norigondolella steinbergensis* | Alaunian-Sevatian | >5.0 |
| 5 | 669836 | 273715 | *Epigondolella slovakensis, Norigondolella steinbergensis, Epigondolella abneptis, Epigondolella* sp. | Alaunian 2 | >5 |
| 8 | 670771 | 270770 | *Paragondolella polygnathiformis* | Carnian (Julian) | 5.0-5.5 |
| | | | **Leckkogel Formation (Late Julian - Early Tuvalian)** | | |
| 6 | 674097 | 274412 | *Paragondolella polignatiformis, Gladigondolella tethydis* | (Cordevolian)-Julian | N.A. |
| 10 | 667727 | 270194 | *Paragondolella polygnathiformis* | Carnian, most probably Julian | >5.0 |
| 12 | 666203 | 270314 | *Gladigondolella tethydis* | Illyrian-Julian | 5.5 |
| 13 | 665694 | 270735 | *Gladigondolella tethydis + ME, Paragondolella polygnathiformis* | (Cordevolian)-Julian | 5.5 |
| | | | **Grafensteig Formation (Late Anisian - Early Carnian)** | | |
| 1 | 664169 | 270653 | *Gladigondolella ME, Paragondolella inclinata* | Longobardian-Julian | 5.5-6.0 |
| 7 | 672829 | 272502 | *Paragondolella excelsa* | Upper Illyrian-Fassanian | 6.0-6.5 |
| | | | **Reifling Formation (Late Anisian)** | | |
| 9a | 668445 | 269919 | *Paragondolella bifurcata, Paragondolella excelsa* | Lower Illyrian | >5.0 |
| 9b | 668449 | 269916 | *Paragondolella bifurcata* | Upper Pelsonian | >5.0 |
| 11 | 666829 | 269854 | *Paragondolella bifurcata, Gladigondolella ME, Neogondolella pseudolonga, Neogondolella constricta* | Upper Pelsonian-Fassanian | 5.0 |

A Horiba Labram HR Evolution instrument, equipped with a 100mW Nd:Yag (532 nm) laser, a confocal microscope (100x/0.7 objective lens, hole aperture=100µm), a 1800 g/mm grating, and a Peltier cooled CCD detector was used to collect Raman spectra. Each spot measurement is an average of two scans (divided in four 20 s accumulations) in the 700–2000 cm−1 region. The band positions were maintained using a silica standard sample. 20 spectra were recorded for the metapelite samples with a laser power filtered to 10 %. Conodont elements were characterized by spot measurements with a laser power filtered to 50 %.

The CM Raman bands were evaluated by the IFORS approach of Lünsdorf and Lünsdorf (2016), excluding subjectivity in curve-fitting (3 repetitions, smooth window size=11, minimum width=20, maximum width=60, minimum distance=5, polynomic baseline of order 2 for the conodont samples, polynomic baseline of order 3 for the metapelite samples, window size= 0.2, alpha= 0.985, sigma threshold = 0.01, noise intensity=1). The obtained results were used to estimate metamorphic temperatures from the regression of the scale total area parameter against metamorphic temperatures of thermometrically well-constrained reference samples (Lünsdorf et al., 2017). To avoid any bias arising from the used sample preparation method and instrumental setting, the reference samples were prepared and analyzed as done with the study samples. The v1-$PO_4^{3-}$ bioapatite band at ca. 963 $cm^{-1}$ was fitted by a linear background and a Lorentzian function using the "Fityk" software of Wojdyr (2010). CAI values were determined visually using a standard set following the classification schemes of Epstein et al. (1977) and Rejebian et al. (1987; see also Gawlick et al., 1994).

## 4 Results

RSCM temperatures estimated from the metapelite samples reconstruct an upright thermal gradient with 380-460 °C in the Veitsch Nappe, ca. 350°C in the Noric Nappe, and 288-313 °C in the Carnian level of the Mürzalpen Nappe (Table 3). In accordance to the temperature calibration of Epstein et al. (1977) and Rejebian et al. (1987), the latter temperature is correlated to CAI values of 5.0-6.5 (Table 1; Figure 2). Conodonts with a CAI>5.5 show specimens with a recrystallized apatite matrix (Figure 2). The Raman spectra of conodont spot measurements show a dominant v1-$PO_4$ apatite band between 953 and 965 $cm^{-1}$ as well as the carbonaceous matter derived D (disorder) and G (graphite) bands (Figure 3). In a singular conodont element, the corresponding metamorphic temperatures vary considerably. If an average is calculated for a sample, significantly higher RSCM temperatures (280-382 °C) than the temperatures of the adjacent slates (288-313 °C) result (Table 3).

## 5 Discussion

The study data compare conventional RSCM temperatures estimated on metapelites (Lünsdorf et al., 2017) to estimates from conodonts (McMillan and Golding, 2019). The RSCM estimates from the metapelites ranging between 290 and 310 °C are based on a lab-specific

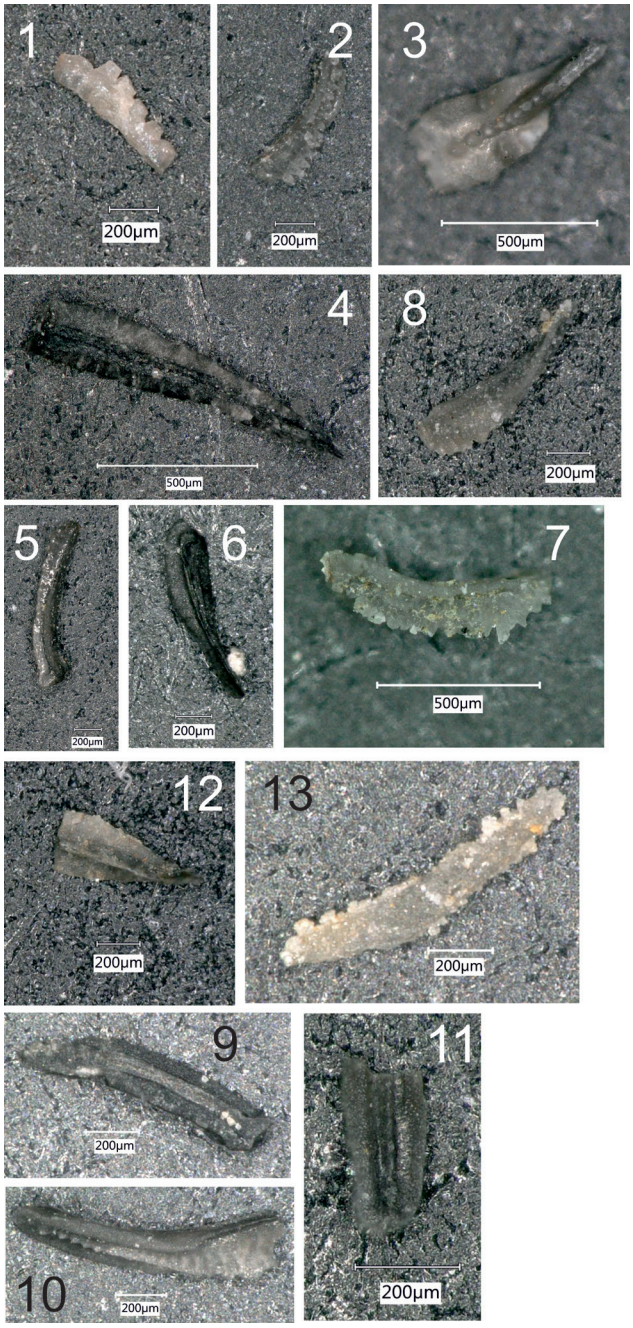


**Figure 2:** Investigated CAI 5.0-6.5 conodonts from the Mürzalpen Nappe (the numbers indicate the sample names, see Table 1). 1. *Gladigondolella* ME. 2. *Paragondolella polygnathiformis*. 3. *Epigondolella rigoi*. 4. *Norigondolella* sp. 5. *Norigondolella steinbergensis*. 6. Basal view on *Paragondolella polygnathiformis*. 7. *Paragondolella excelsa*. 8. *Paragondolella polygnathiformis*. 9. *Paragondolella bifurcata*. 10. *Paragondolella polygnathiformis*. 11. Broken piece of *Neogondolella pseudolonga*, basal view. 12. Broken piece of *Gladigondolella* sp. 13. Totally recrystallized *Gladigondolella tethydis*. The specimens shown in 1, 7, and 13 show a recrystallized apatite matrix.

calibration, established by data from samples with well-constrained peak temperatures (Lünsdorf et al., 2017; Rantitsch et al., 2020). Therefore, they are used here as a reference and correlated to CAI values of 5.0-6.5.

The spectral characteristics (i.e. band position and band full width at half maximum, FWHM) of the $v_1$-$PO_4$ apatite band at ca. 963 $cm^{-1}$ provide evidence for diagenetic alteration (Lanfranco et al., 2003; Thomas et al. 2007, 2011; McMillan and Golding, 2019; McMillan et al. 2019). According to Zhang et al. (2017), a parameter scatterplot identifies a Sr, $CO_3^{2-}$ or F- substitution into the recrystallized conodont apatite. In a thermometric study, McMillan and Golding (2019) found that conodonts for which IFORS and CAI temperatures do not match show more evidence for diagenetic cation replacement. The data of this study demonstrate a strong negative correlation between v1-$PO_4$ apatite band position and FWHM (Figure 4), suggesting varying contents of a heavier cation (Thomas et al., 2011). Conodont spot measurements revealing RSCM temperatures equal to the RSCM reference temperatures are characterized by relatively broad v1-$PO_4$ bands (high FWHM values) shifted to lower wavenumbers. According to Thomas et al. (2011) and Zhang et al. (2017 and references therein), those spots show a higher substituting ion concentration in the lattice. RSCM temperatures estimated on spots characterized by lower substituting ion concentrations are shifted to values significantly higher than the reference slate temperatures (Figure 5). Consequently, evidence is given for a post-diagenetic alteration or overgrowth of the conodont apatite, which lowers a previously high substituting lattice concentration. The v1-$PO_4$ band parameter vary in a singular conodont as well as between distinct conodont specimens of a sample, evidencing a heterogeneous process, detected in the entire CAI range covered by this study (5.0-6.5).

The results suggest that chemical alteration and recrystallization must be considered in the application of RSCM on the conodonts of this study. Without assessment of the v1-$PO_4$ band characteristics, an average temperature is biased towards higher values. The best value is found however at the bulk minimum of the data collection. Unbiased estimates are found at spots with an apatite parameter combination of band positions < 956 $cm^{-1}$ and FWHM > 12 $cm^{-1}$. However, sample 2 gives an average temperature estimate corresponding to the slate estimates (Table 3) outside those limits. This is related to a differing starting composition of the conodont apatite or by a thermal overprint at a lower temperature than the reference range.

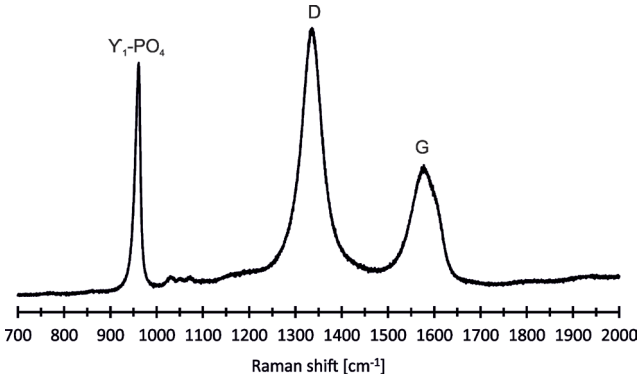


**Figure 3:** Representative conodont Raman spectrum of a spot measurement of sample 5. The $v_1$-$PO_4$ band derives from apatite, the D (disorder) and G (graphite) bands derive from carbonaceous material.

**Table 2:** Metapelite samples (coordinates in the Austrian BMN system, EPSG 31286).

| Sample | X | Y |
|---|---|---|
| **MürztalNappe (LeckkogelFormation, Carnian)** | | |
| 14 | 666419 | 270867 |
| 15 | 666369 | 270659 |
| 16 | 666473 | 270340 |
| 17a | 666887 | 269948 |
| 17b | 666866 | 269933 |
| 18 | 673336 | 272613 |
| 19 | 674192 | 274503 |
| **NoricNappe (Rad Formation, Silurian)** | | |
| 20 | 665813 | 268707 |
| **Veitsch Nappe (SunkFormation, Upper Carboniferous)** | | |
| 21 | 666386 | 265399 |
| 22a | 667658 | 265468 |
| 22b | 667648 | 265478 |
| 23 | 666218 | 265175 |

Because of the regionally consistent zonation of the reference temperatures, the latter interpretation is excluded, giving evidence for the importance to consider the apatite structure in thermometric conodont studies. Consequently, to estimate reliable temperatures, the alteration of the host apatite has to be assessed by an inspection of the $v_1$-$PO_4$ band characteristics (Figure 5). Valid temperatures (corrected temperatures of Table 3) are given by the median of all spot measurements limited by the apatite parameter combination defined above. However, it is also obvious that some samples do not allow to estimate accurate temperatures (Table 3).

The high substituting ion concentration in the apatite lattice could be explained by a chemically abnormal environment during deposition and/or early diagenesis or by a later alteration of the host carbonates. As the apatite characteristics do not vary in time and facies (Table 3), the first explanation seems unlikely. In contrast, there is some evidence for the latter hypothesis: Firstly, there is geochemical evidence for a significant brine-rock alteration. Invasion of highly fractionated hypersaline fluids in Late Triassic times triggered magnesite mineralization in the Veitsch Nappe and siderite mineralization in the Noric Nappe (Prochaska, 2016), tectonically below the conodont host rocks. Later, syntectonic fluids moved during incipient metamorphism of the Haselgebirge evaporites (Spötl et al., 1996, 1998 a, b, 1999). Secondly, in the central Northern Calcareous Alps, limestone samples show extraordinarily high Sr concentrations, pointing to a spatially inhomogeneous redistribution process (Kralik and Schramm, 1994). Thus, it is possible that hydrothermal activity was responsible for a considerable Sr enrichment of the conodont surface. In a preliminary model, recrystallization removed Sr ions out of the lattice. Thus, the $v_1$-$PO_4$ band characteristics may provide a proxy for the stress of growing apatite crystals, promoting an accelerated graphitization of the involved carbonaceous matter.

The regional significance of the study data is given by the observation of a continuous metamorphic trend across nappe boundaries. From bottom to top, ca. 400 °C are estimated in the Veitsch Nappe, 350 °C in the Noric Nappe and 300°C in the Carnian level of the Mürzalpen Nappe. Published data from the Permian-Lower Triassic Haselgebirge of max. 255-360° (Spötl and Hasenhüttl, 1998; Bojar et al., 2018) fit well into this gradient. The age of metamorphism in the Greywacke Zone is early Late Cretaceous (Dallmeyer et al., 1998; Frank and Schlager, 2006) but uncertain in the Mürzalpen Nappe. Because of an insufficient overburden thickness (Bryda et al., 2013, 2020), however, only tectonic load can explain the high thermal overprint of the Triassic strata.

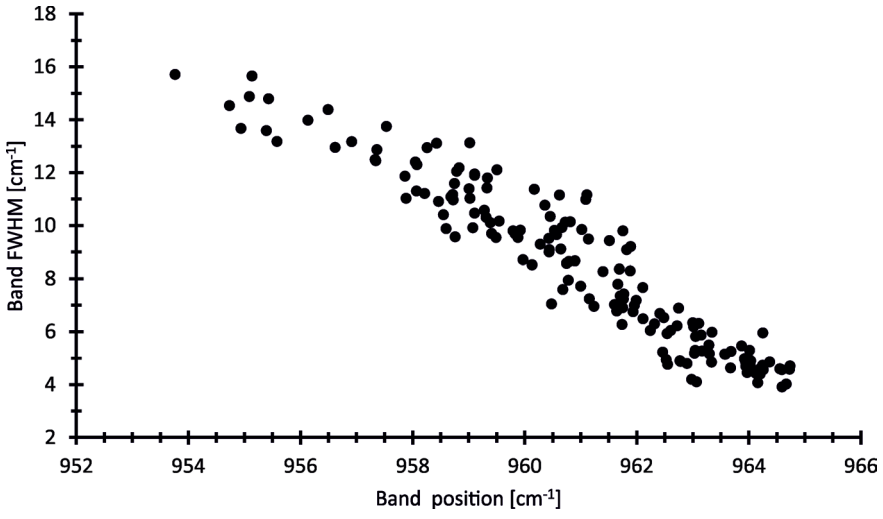


**Figure 4:** Relationship between band width (FWHM= full width at half maximum) and position of the v1-$PO_4$ band as estimated on 180 conodont spot locations (all recorded spot data are shown). The covariation indicates a continuous variation of the substituting ion concentration in the apatite lattice (Thomas et al., 2011).

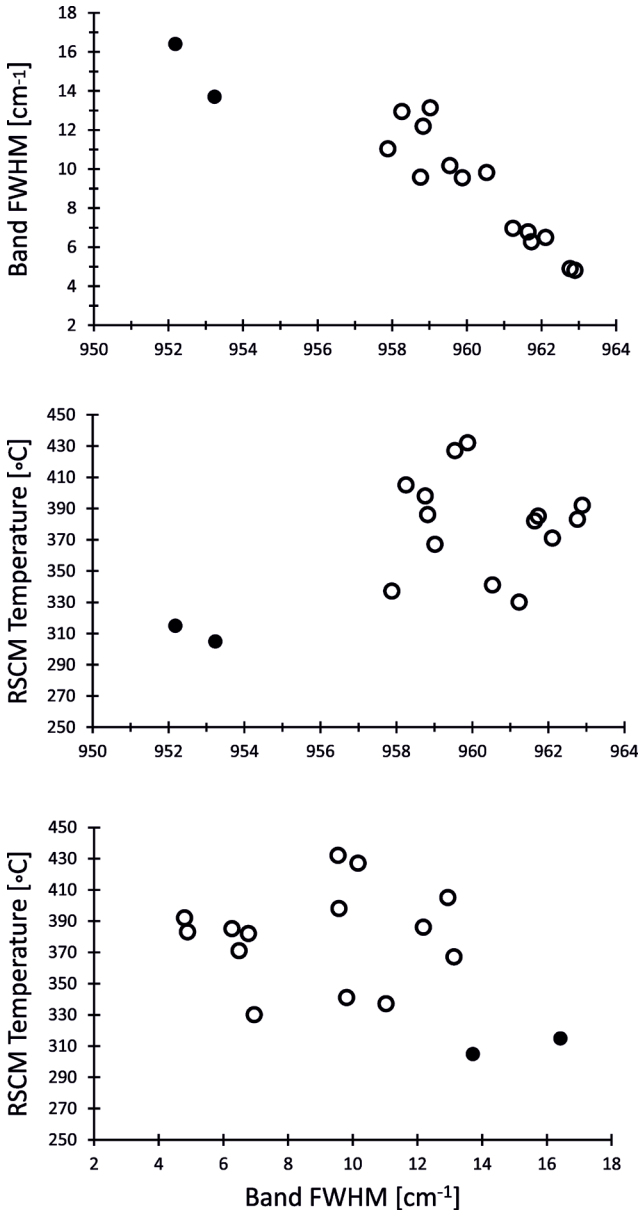


**Figure 5:** Representative example showing the apatite band parameters of the conodont sample 5. Reliable RSCM temperature estimates (full circles) are recorded by spot measurements with a $\nu_1$-$PO_4$ parameter combination of band center < 956 $cm^{-1}$ and band FWHM > 12$cm^{-1}$ (corrected temperatures of Table 3).

**Table 3:** RSCM temperature estimates according to Lünsdorf et al. (2017). Temp= RSCM temperature, +/-= 0.9 temperature confidence, Nc conodonts= number of analyzed conodonts, Nm= number of measurements, corrected Temp= peak temperature by considering apatite alteration.

| Sample | Nc | Nm | Temp[°C] | +/- | corrected Temp [°C] |
|---|---|---|---|---|---|
| **MürztalNappe (Carbonates)** | | | | | |
| 1 | 3 | 7 | 280 | 83 | <322 |
| 2 | 2 | 10 | 303 | 31 | 300 |
| 3 | 6 | 16 | 364 | 32 | <366 |
| 4 | 7 | 21 | 363 | 32 | 286 |
| 5 | 6 | 17 | 382 | 38 | 310 |
| 6 | 2 | 10 | 369 | 32 | <329 |
| 7 | 5 | 13 | 364 | 32 | <376 |
| 8 | 6 | 18 | 355 | 32 | 315 |
| 9a | 6 | 15 | 358 | 32 | <342 |
| 9b | 6 | 15 | 336 | 38 | 315 |
| 10 | 1 | 5 | 366 | 32 | <366 |
| 11 | 5 | 16 | 335 | 32 | 299 |
| 12 | 1 | 5 | 357 | 32 | 338 |
| 13 | 4 | 12 | 368 | 32 | <351 |
| **MürztalNappe (Metapelites)** | | | | | |
| 14 | | 20 | 288 | 31 | |
| 15 | | 20 | 288 | 31 | |
| 16 | | 20 | 302 | 31 | |
| 17a | | 20 | 306 | 31 | |
| 17b | | 20 | 313 | 32 | |
| 18 | | 20 | 295 | 31 | |
| 19 | | 20 | 304 | 31 | |
| **NoricNappe (Rad Formation, Silurian)** | | | | | |
| 20 | | 20 | 351 | 32 | |
| **Veitsch Nappe (SunkFormation, UpperCarboniferous)** | | | | | |
| 21 | | 20 | 420 | 38 | |
| 22a | | 20 | 381 | 32 | |
| 22b | | 20 | 404 | 33 | |
| 23 | | 20 | 460 | 29 | |

## 6 Conclusions

Raman Spectroscopy on conodonts and metapelites of the Mürzalpen Nappe (Northern Calcareous Alps) and its basement allow to draw both methodological and regional conclusions:

1) Raman spectroscopy on carbonaceous material of Triassic conodonts of the Mürzalpen Nappe yields higher metamorphic temperatures than estimates from adjacent metapelites. This is explained by an enhanced graphitization due to recrystallization of the apatite matrix. The data confirm the fact that it is necessary to assess the chemical and structural state of the conodonts to estimate accurate RSCM temperatures. For this purpose, the v1-$PO_4$ apatite band characteristics can be used.

2) In the Northern Calcareous Alps, CAI values of 5.0-6.5, representative for large segments of the Juvavic Nappe System (Gawlick et al., 1994), correlate to ca. 300°C.

3) The thermal overprint of Anisian to Norian carbonates of the Juvavic Mürzalpen Nappe is related to thrust tectonics and tectonic load in the frame of the destruction of the Austroalpine Neo-Tethys continental margin.

## Acknowledgements

We acknowledge Ch. Iglseder and M.S. Hollinetz for providing samples from the Greywacke Zone. Special thanks to L. Krystyn for independently confirming the conodont determinations. We thank also Franz Neubauer and an anonymous reviewer for their comments and Sylke Hilberg for the editorial work.

**References**


Bojar, A.-V., Halas, S., Bojar, H.-P., Trembaczowski, A., 2018. Late Permian to Triassic isotope composition of sulfates in the Eastern Alps: palaeogeographic implications. Geological Magazine, 155, 797–810. https://doi.org/10.1017/S0016756816000996

Bryda, G., van Husen, D., Kreuss, O., Koukal, V., Moser, M., Pavlik, O., Schönlaub, H.P., Wagreich, M., 2013. Geologische Karte der Republik Österreich 1:50000, Erläuterungen zu Blatt 101 Eisenerz. Geologische Bundesanstalt Wien, 230 pp.

Bryda, G., Ćorić, S., Van Husen, D., Kreuss, O., Mandl, G.W., Pavlik, W., Reiser, M., Moser, M., 2020. Geologische Karte der Republik Österreich. Blatt 102 Aflenz Kurort. Geologische Bundesanstalt Wien. 1:50000, in print.

Budurov, K.J., Sudar, M.N., 1990. Late Triassic Conodont Stratigraphy. In: Ziegler, W. (ed.), Papers on Conodonts and Ordovician to Triassic Conodont Stratigraphy. Contribution IV, Courier Forschunginstitut Senckenberg, 118, pp 203-239.Chen, Y., Krystyn, L., Orchard, M.J., Lai, X.-L., Richoz, S., 2016. A review of the evolution, biostratigraphy, provincialism and diversity of Middle and Late Triassic conodonts. Papers in Palaeotonlogy, 2, 235-263. https://doi.org/10.1002/spp2.1038

Chen, Y., Krystyn, L., Orchard, M.J., Lai, X.-L., Richoz, S., 2016. A review of the evolution, biostratigraphy, provincialism and diversity of Middle and Late Triassic conodonts. Papers in Palaeotonlogy, 2, 235-263. https://doi.org/10.1002/spp2.1038

Dallmeyer, R.D., Handler, R., Neubauer, F., Fritz, H., 1998. Sequence of thrusting within a thick- skinned tectonic wedge: evidence from 40Ar/39Ar and Rb-Sr ages from the Austroalpine Nappe complex of the Eastern Alps. The Journal of Geology, 106, 71–86. https://doi.org/10.1086/516008

Epstein, A.G., Epstein, J.B., Harris, L.D., 1977. Conodont Color Alteration Index to Organic Metamorphism. Geological Survey Professional paper, 995, 1–27.

Frank, W., Schlager W., 2006. Jurassic strike slip versus subduction in the Eastern Alps. Geologische Rundschau, 95, 431-450. https://doi.org/10.1007/s00531-005-0045-7

Frisch, W., Gawlick, H.J., 2003. The nappe structure of the central Northern Calcareous Alps and its disintegration during Miocene tectonic extrusion—A contribution to understanding the orogenic evolution of the eastern Alps: International Journal of Earth Sciences, 92, 712–727. https://doi.org/10.1007/s00531-003-0357-4

Frühauf, S., 2017. Thermometrie an Erzen und Nebengesteinen der Sideritlagerstätte Steirischer Erzberg. Bachelor thesis, Montanuniversität Leoben, Austria, 59 pp.

Gallet, Y., Krystyn, L., Besse, J., 1998. Upper Anisian to Lower Carnian magnetostratigraphy from the Northern Calcareous Alps. Journal of Geophysical Research, 103, 605–621. https://doi.org/10.1029/97JB02155

Gawlick, H.-J., Krystyn, L., Lein, R., 1994. Conodont colour alteration indices: Palaeotemperatures and metamorphism in the Northern Calcareous Alps - a general view. Geologische Rundschau, 83, 660–664.

Gawlick, H.-J., Frisch, W., Vecsei, A., Steiger, T., Böhm, F., 1999. The change from rifting to thrusting in the Northern Calcareous Alps as recorded in Jurassic sediments. Geologische Rundschau, 87, 644–657. https://doi.org/10.1007/s005310050237

Haas, I., Eichinger, S., Haller, D., Fritz, H., Nievoll, J., Mandl, M., Hippler, D., Hauzenberger, C., 2020. Gondwana fragments in the Eastern Alps: A travel story from U/Pb zircon data. Gondwana Research, 77, 204–222. https://doi.org/10.1016/j.gr.2019.07.015

Kralik, M., Schramm, J.-M., 1994. Illit-Wachstum: Übergang Diagenese - Metamorphose in Karbonat- und Tongesteinen der Nördlichen Kalkalpen: Mineralogie und Isotopengeologie (Rb-Sr, K-Ar und C-O). Jahrbuch der Geologischen Bundesanstalt, 137, 105–137.

Kralik, M., Krumm, H., Schramm, J.-M., 1987. Low grade and very low grade metamorphism in the Northern Calcareous Alps and in the Greywacke Zone: Illite - Crystallinity data and isotopic ages. In: Flügel, H.W., Faupl, P. (eds.), Geodynamics of the Eastern Alps. F. Deuticke, Wien, pp. 164–178.

Krystyn, L., Mandl, G.W., Schauer, M., 2009. Growth and termination of the Upper Triassic platform margin of the Dachstein area (Northern Calcareous Alps, Austria). Austrian Journal of Earth Sciences, 102, 23–33.

Lanfranco, A. M., Schofield, P. F., Murphy, P. J., Hodson, M. E., Mosselmans, J. F. W., Valsami-Jones, E. (2003). Characterization and identification of mixed-metal phosphates in soils: the application of Raman spectroscopy. Mineralogical Magazine, 67, 1299–1316. https://doi.org/10.1180/0026461036760166

Lein, R., 2010. Die Entwicklung des Karnbeckens von Aflenz im Spannungsfeld zwischen Eustatik und synsedimentärer Tektonik (Nördliche Kalkalpen, Österreich). Journal of Alpine Geology, 53, 181–199.

Lein, R., Gawlick, H.-J., 2001. Neue Grundlagen zur tektonischen Interngliederung der Mürzalpendecke auf der Basis von Conodont Colour Alteration Index (CAI)-Untersuchungen. Arbeitstagung der Geologischen Bundesanstalt 2001, Neuberg an der Mürz, 132–134.

Leitner, C., Neubauer, F., Genser, J., Borojević-Šoštarić, S., Rantitsch, G., 2014. 40Ar/39Ar ages of crystallization and recrystallization of rock-forming polyhalite in Alpine rocksalt deposits. Geological Society, London, Special Publications, 378, 207–224. http://dx.doi.org/10.1144/SP378.5

Linzer, H.-G., Ratschbacher, L., Frisch, W., 1995. Transpressional collision structures in the upper crust: the fold-thrust belt of the Northern Calcareous Alps. Tectonophysics, 242, 41–61. https://doi.org/10.1016/0040-1951(94)00152-Y

Lünsdorf, N.K., Lünsdorf, J.O., 2016. Evaluating Raman spectra of carbonaceous matter by automated, iterative curve-fitting. International Journal of Coal Geology, 160–161, 51–62. http://dx.doi.org/10.1016/j.coal.2016.04.008

Lünsdorf, N.K., Dunkl, I., Schmidt, B.C., Rantitsch, G., von Eynatten, H., 2017. Towards a higher comparability of

geothermometric data obtained by Raman spectroscopy of carbonaceous material. Part 2: A revised geothermometer. Geostandards and Geoanalytical Research, 41, 593–612. https://doi.org/10.1111/ggr.12178

Mandl, G.W., 2000. The Alpine sector of the Tethyan shelf - Examples of Triassic to Jurassic sedimentation and deformation from the Northern Calcareous Alps. Mitteilungen der österreichischen geologischen Gesellschaft, 92, 61–77.

Mandl, G.W., 2001. Zum tektonischen Bauplan der östlichen Kalkhochalpen. Arbeitstagung der Geologischen Bundesanstalt 2001, Neuberg an der Mürz, 123–131.

Marshall, C.P., Mar, G.L., Nicoll, R.S., Wilson, M.A., 2001. Organic geochemistry of artificially matured conodonts. Organic Geochemistry, 32, 1055–1071. https://doi.org/10.1016/S0146-6380(01)00077-8

McMillan, R., Golding, M., 2019. Thermal maturity of carbonaceous material in conodonts and the Color Alteration Index: Independently identifying maximum temperature with Raman spectroscopy. Palaeogeography, Palaeoclimatology, Palaeoecology, 534, 109290. https://doi.org/10.1016/j.palaeo.2019.109290

McMillan, R., Snoeck, C., Winter, N. J. de, Claeys, P., Weis, D. 2019. Evaluating the impact of acetic acid chemical pre-treatment on 'old' and cremated bone with the 'Perio-spot' technique and 'Perios-endos' profiles. Palaeogeography, Palaeoclimatology, Palaeoecology. 530, 330–344. https://doi.org/10.1016/j.palaeo.2019.05.019

Medici, L., Malferrari, D., Savioli, M., Ferretti, A., 2020. Mineralogy and crystallization patterns in conodont bioapatite from first occurrence (Cambrian) to extinction (end-Triassic). Palaeogeography, Palaeoclimatology, Palaeoecology, 549, 109098. https://doi.org/10.1016/j.palaeo.2019.02.024

Neubauer, F., Handler, R., Hermann, S., Paulus, G., 1994. Revised lithostratigraphy and structure of the Eastern Greywacke Zone (Eastern Alps). Mitteilungen der Österreichischen Geologischen Gesellschaft, 86, 61–74.

Noyan, Ö.F., Kozur, H.W., 2007. Revision of the late Carnian – early Norian conodonts from the Stefanion section (Argolis, Greece) and their palaeobiogeographic implications. – Neues Jahrbuch für Geologie und Paläontologie, Abhandlungen, 245, 159–178.

Orchard, M.J., 2010. Triassic conodonts and their role in stage boundary definition. Geological Society, London, Special Publications, 334, 139–161. https://doi.org/10.1144/SP334.7

Prochaska, W. (2016). Genetic concepts on the formation of the Austrian magnesite and siderite mineralizations in the Eastern Alps of Austria. Geologia Croatica, 69, 31–38. https://doi.org/10.4154/gc.2016.03

Pucéat, E., Reynard, B., Lécuyer, C., 2004. Can crystallinity be used to determine the degree of chemical alteration of biogenic apatites? Chemical geology, 205, 83–97. https://doi.org/10.1016/j.chemgeo.2003.12.014

Rantitsch, G., Russegger, B., 2005. Organic maturation within the central Northern Calcareous Alps (Eastern Alps). Austrian Journal of Earth Sciences, 98, 68–76.

Rantitsch, G., Grogger, W., Teichert, C., Ebner, F., Hofer, C., Maurer, E.-M., Schaffer, B., Toth, M., 2004. Conversion of carbonaceous material to graphite within the Greywacke Zone of the Eastern Alps. International Journal of Earth Sciences, 93, 959–973. https://doi.org/10.1007/s00531-004-0436-1

Rantitsch, G., Iglseder, C., Schuster, R., Hollinetz, M. S., Huet, B., Werdenich, M., 2020. Organic metamorphism as a key for reconstructing tectonic processes: a case study from the Austroalpine unit (Eastern Alps). International Journal of Earth Sciences, 109, 2235–2253. https://doi.org/10.1007/s00531-020-01897-7

Ratschbacher, L., 1987. Stratigraphy, tectonics and paleogeography of the Veitsch nappe (Graywacke zone, Eastern Alps: A rearrangement. In: Flügel, H.W., Sassi, F.P., Grecula P. (eds.), Pre-Variscan and Variscan events in the Alpine-Mediterranean mountain belts. Alfa, Bratislava, pp. 407–414.

Rejebian, V.A., Harris, A.G., Huebner, J.S., 1987. Conodont color and textural alteration: An index to regional metamorphism, contact metamorphism, and hydrothermal alteration. Geological Society of America Bulletin, 99, 471–479.

Sachsenhofer, R.F., Bechtel, A., Reischenbacher, D., Weiss, A., 2003. Evolution of lacustrine systems along the Miocene Mur-Mürz fault system (Eastern Alps, Austria) and implications on source rocks in pull-apart basins. Marine and Petroleum Geology. 20, 83–110. https://doi.org/10.1016/S0264-8172(03)00018-7

Schmid, S.M., Fügenschuh, B., Kissling, E., Schuster, R., 2004. Tectonic map and overall architecture of the Alpine orogen. Eclogae Geologicae Helvetiae, 97, 93–117. https://doi.org/10.1007/s00015-004-1113-x

Schramm, J.-M., 1982. Zur Metamorphose des feinklastischen Permoskyth im Ostabschnitt der Nördlichen Kalkalpen (Ostösterreich). Verhandlungen der Geologischen Bundesanstalt, 1982, 63–72.

Schuster, R., Frank, W., 1999. Metamorphic evolution of the Austroalpine units east of the Tauern Window: indications for Jurassic strike slip tectonics. Mitteilungen der Gesellschaft der Geologie und Bergbaustudenten Österreichs, 42, 37–58.

Schuster, R., Nowotny, A., 2015. Die Einheiten des Ostalpinen Kristallins auf den Kartenblättern GK50 Blatt 103 Kindberg und 135 Birkfeld. Arbeitstagung der Geologischen Bundesanstalt 2015, Mitterdorf im Mürztal 10–37.

Spötl, C., Hasenhüttl, C., 1998. Thermal history of the evaporitic Haselgebirge mélange in the Northern Calcareous Alps (Austria). Geologische Rundschau, 98, 449–460.

Spötl, C., Kralik, M., Kunk, M.J., 1996. Authigenic feldspar as an indicator of paleo-rock/water interactions in Permian carbonates of the Northern Calcareous Alps, Austria. Journal of Sedimentary Research, 66, 139–146.

Spötl, C., Kunk, M.J., Ramseyer, K., Longstaffe, F.J., 1998a. Authigenic potassium feldspar - a tracer for the timing of paleo-fluid flow in carbonate rock, Northern Calcareous Alps, Austria. In: Parnell, J. (ed.), Dating and duration

of fluid flow and fluid-rock interaction. Geological Society of London Special Publications, 144, 107–128.

Spötl, C., Longstaffe, F.J., Ramseyer, K., Kunk, M.J., Wiesheu, R., 1998b. Fluid-rock reactions in an evaporitic mélange, Permian Haselgebirge, Austrian Alps. Sedimentology, 45, 1019–1044.

Spötl, C., Longstaffe, F.J., Ramseyer, Rüdinger, B., 1999. Authigenic albite in carbonate rocks - a tracer for deep-burial brine migration? Sedimentology, 46, 649–666.

Thomas, D.B., Fordyce, R.E., Frew, R.D., Gordon, K.C., 2007. A rapid, non-destructive method of detecting diagenetic alteration in fossil bone using Raman spectroscopy. Journal of Raman Spectroscopy. 38, 1533–1537. https://doi.org/10.1002/jrs.1851

Thomas, D.B., McGoverin, C.M., Fordyce, R.E., Frew, R.D., Gordon, K.C., 2011. Raman spectroscopy of fossil bioapatite — A proxy for diagenetic alteration of the oxygen isotope composition. Palaeogeography, Palaeoclimatology, Palaeoecology, 310, 62–70. https://doi.org/10.1016/j.palaeo.2011.06.016

Trotter, J.A., Eggins, St.M., 2006. Chemical systematics of conodont apatite determined by laser ablation ICPMS. Chemical Geology, 233, 196-216. http://dx.doi.org/10.1016/j.chemgeo.2006.03.004

Wojdyr, M., 2010. Fityk: a general-purpose peak fitting program. Journal of applied crystallography, 43, 1126–1128.

Zhang, L., Cao, L., Zhao, L., Algeo, T.J., Chen, Z.-Q., Li, Z., Lv, Z., Wang, X., 2017. Raman spectral, elemental, crystallinity, and oxygen-isotope variations in conodont apatite during diagenesis. Geochimica et Cosmochimica Acta, 210, 184–207. http://dx.doi.org/10.1016/j.gca.2017.04.036

Received: 20.7.2020
Accepted: 30.9.2020
Editorial Handling: Sylke Hilberg